Characterization of Second-Harmonic Effects in IMPATT Diodes

By C. A. BRACKETT

(Manuscript received May 20, 1970)

We discuss characterization of the tuned-harmonic mode of operation in IMPATT oscillators, and introduce an equivalent circuit which incorporates the large-signal, "single-frequency" oscillator admittances at the fundamental and second-harmonic frequencies. Complete characterization of this mode is equivalent to specifying the behavior of each of the four elements of the equivalent circuit as functions of the oscillation state variables: fundamental voltage and frequency, second-harmonic voltage and relative phase. Using the approximate large-signal analysis of Blue,[1] the values of the equivalent circuit elements are presented, as an example, for a 6-GHz IMPATT diode under a variety of oscillation conditions. This equivalent circuit is used to clarify the role played by the fundamental and second-harmonic, single-frequency oscillator admittances in the tuned-harmonic mode.

Using an approximation to the equivalent circuit, we investigate the criteria for stable oscillation of the tuned-harmonic mode. It is found that the stability criteria are in general quite restrictive. For the same 6-GHz germanium diode, the range of stable phase is investigated, as a function of the RF parameters, for certain special cases. It is found to be possible to satisfy the stability criteria for the phase which gives an optimum enhancement of the fundamental power output if certain conditions on the external RF circuit are satisfied.

I. INTRODUCTION

It was found by Swan[2] that the introduction of a trapped resonance at the second harmonic of the oscillation frequency in a 6-GHz Ge IMPATT diode oscillator provided dramatic increases in the output power and efficiency, as compared with the results obtained with the ordinary single quarter-wave transformer coaxial circuit. Since that time several authors[1,3–8] have reported both theoretical and experi-

mental examinations of the effect. It appears that the addition of a properly phased second-harmonic voltage improves the phasing of the RF current relative to the fundamental voltage so as to increase the negative conductance and (at least at lower frequencies) give an increase in the power output at the fundamental frequency. The circuit conditions required for the observation of this effect have been incompletely understood.

The purpose of this paper is to present the results of an analytical study of the interaction of an IMPATT diode with a circuit having resonances at two harmonically related frequencies. The analysis is begun by the introduction of an equivalent circuit for the diode by which these two-frequency oscillators may be characterized. A stability theory is then developed along the lines taken by Kurokawa which examines whether a particular circuit, even though matching the impedances required by the diode at both frequencies, will or will not provide a stable oscillation.[9,10] The stability theory is examined in some generality, and three special cases are studied for which tractable analytical results can be obtained. It is found that in the case of zero fundamental or second-harmonic voltage, the theory reduces to the single-frequency stability criteria derived by Kurokawa. In more general cases, the theory indicates that by designing (or adjusting) the circuit carefully one can obtain stable operation at phase angles which enhance the fundamental power. However, the theory also indicates that stable operation may be impossible if the circuit-diode interaction is not just right, even though the diode and circuit are matched to each other at the two frequencies.

In a final section, a numerical example is given in which the theory is applied to a model of a 6-GHz germanium IMPATT diode, using the approximate large-signal analysis of Blue.[1]

II. TWO-FREQUENCY CHARACTERIZATION

The IMPATT oscillator is truly a single-frequency oscillator only at very small ac voltages and currents. At larger signal levels the nonlinearity is very strong, and therefore there should be strong interactions between harmonically related signals. However, by operating the diode in a well-designed single-frequency circuit, the power output may be limited to a single frequency. This may be done, for example, by presenting short-circuit, open-circuit, or reactive loads at the harmonic frequencies. In the case of short circuited harmonics, the harmonic voltage amplitudes V_k are zero, and only the fundamental voltage V_1 is nonzero. It is then common practice to calculate a large-

signal diode admittance as a function of V_1 and to use this admittance to describe device behavior. On the other hand, for the case of open-circuited harmonics, the harmonic currents, I_k are zero, and only the fundamental current I_1 is nonzero. It is then preferable to characterize the diode by a large-signal impedance which is a function of the RF current amplitude I_1. Both of these conditions constitute tunings at the harmonic frequencies, albeit ones that are particularly useful and simple to express analytically.

To consider other, more general, loading conditions at the harmonic frequencies, one must introduce two more variables (amplitude and phase) for each additional frequency for which the amplitude is nonzero. One of the most important points is that the input admittance (for example) at the fundamental frequency is no longer a unique function of V_1 and the frequency f; but instead defining the state of oscillation requires a vector whose components are $V_1, \cdots, V_N, f, \varphi_2, \cdots, \varphi_N$ where N is the maximum harmonic number of interest and φ_k is the phase of the kth harmonic voltage relative to the fundamental. This vector does uniquely describe the state of oscillation, and for every such vector, there exists a set of complex admittances $y_1 \cdots y_N$ which are uniquely determined. If this is not so, it simply means we have inadequately described the system and must include more component signals, either harmonics or subharmonics.

We shall limit the discussion to include only two harmonically related frequencies and consider that $V_k = 0$ for $k > 2$. This also means that we will only discuss the admittance characterization and not the impedance characterization.

A convenient way of utilizing the information already known about the large-signal single-frequency admittance of the diode is to separate the input admittances at the two frequencies as shown in Fig. 1. This equivalent circuit shows a fundamental port and a second-harmonic

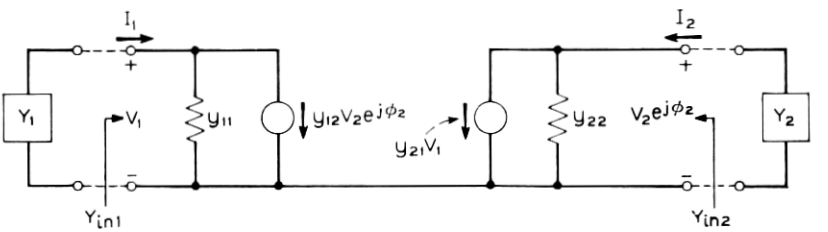

Fig. 1—Equivalent circuit of the IMPATT diode which includes nonzero voltages at two harmonically related frequencies. Port 1 is the fundamental port and port 2 is the second-harmonic port; y_{11} and y_{22} are the large-signal single-frequency diode admittances at the fundamental and second-harmonic frequencies, respectively.

port. The admittances $y_{11}(V_1)$ and $y_{22}(V_2)$ are the large-signal single-frequency admittances that would be measured at the fundamental if there were no harmonic (or subharmonic) voltages present. That is, they are just the ordinary large-signal admittances $y(V)$ at the frequencies f and $2f$.

The admittances $y_{12}(V_1, V_2, f, \varphi_2)$ and $y_{21}(V_1, V_2, f, \varphi_2)$ account for the conversion of current between the two frequencies and it is the study of their effects that is the main subject of this paper. The phase φ_2 is defined by the assumed voltage waveforms

$$v_1(t) = V_1 \cos \omega_0 t$$

and

$$v_2(t) = V_2 \cos (2\omega_0 t + \varphi_2).$$

The input admittances are

$$Y_{in1} = y_{11} + y_{12} \frac{V_2 \exp (j\varphi_2)}{V_1} \tag{1}$$

and

$$Y_{in2} = y_{22} + y_{21} \frac{V_1}{V_2 \exp (j\varphi_2)} \tag{2}$$

at the fundamental and second-harmonic frequencies respectively. Since y_{11} and y_{22} are independent of the phase φ_2 by definition, equations (1) and (2) show that the input admittance loci for fixed V_1 and V_2 will be counter rotating closed curves as a function of φ_2. These curves will enclose the admittance points y_{11} and y_{22} separately providing that y_{12} and y_{21} are not strong functions of φ_2. If, for example, y_{12} and y_{21} are independent of φ_2, Y_{in1} and Y_{in2} will be circles centered about y_{11} and y_{22} respectively, the radii of which depend upon the ratio V_2/V_1. They generally turn out to be somewhat elliptical in shape[8] although, in many cases, of very low eccentricity.

Figure 2 is the calculated[1] large-signal, single-frequency, admittance plane plot for a 6-GHz germanium diode, from which y_{11} and y_{22} may be obtained directly. Figures 3 and 4 show Y_{in1} and Y_{in2} for various fundamental frequencies when the voltages are held constant, demonstrating the elliptical and circular behavior noted above. Note that in Fig. 4 the second-harmonic input admittance has a positive real part for some ranges of the phase φ_2. To operate at such phase angles and RF voltages, the external circuit must supply power to the diode at the second-harmonic frequency, and thus these conditions are un-

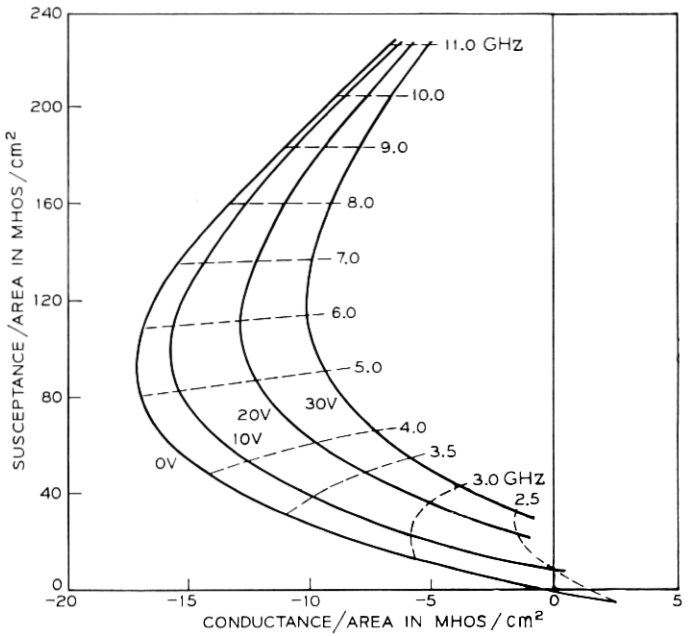

Fig. 2—The calculated large-signal single-frequency admittance of a 6-GHz germanium IMPATT diode at a bias current density $J_0 = 340$ A/cm².

realizable when operating into a passive circuit. The diameter of these admittance contours is inversely proportional to the second-harmonic voltage amplitude V_2, however, so that at higher values of V_2, the entire contour may lie in the left-half plane.

The rather simple structure of the Y_{in1} and Y_{in2} loci of Figs. 3 and 4 suggests that y_{12} and y_{21} might be rather insensitive functions of φ_2. This is borne out by the plots of Fig. 5 in which y_{12} and y_{21} are shown at constant fundamental voltage V_1 and several values of V_2, with φ_2 ranging $0 \leqq \varphi_2 \leqq 2\pi$. This figure also establishes that y_{12} and y_{21} do not change drastically as a function of V_2. It was also found that y_{12} and y_{21} depend upon V_1 in an approximately linear fashion. This is shown in Fig. 6 where y_{12}/V_1 and y_{21}/V_1 are plotted versus V_1 for several values of φ_2 with V_2 constant. Thus, for moderate values of V_1 and V_2, we can make the approximation that y_{12} and y_{21} are both proportional to V_1 and independent of φ_2 and V_2. To demonstrate this analytically, let the phase of the fundamental voltage $\varphi_1 \neq 0$, and consider a power series expansion of the currents $i_{12} = y_{12}V_2 \exp(j\varphi_2)$ and

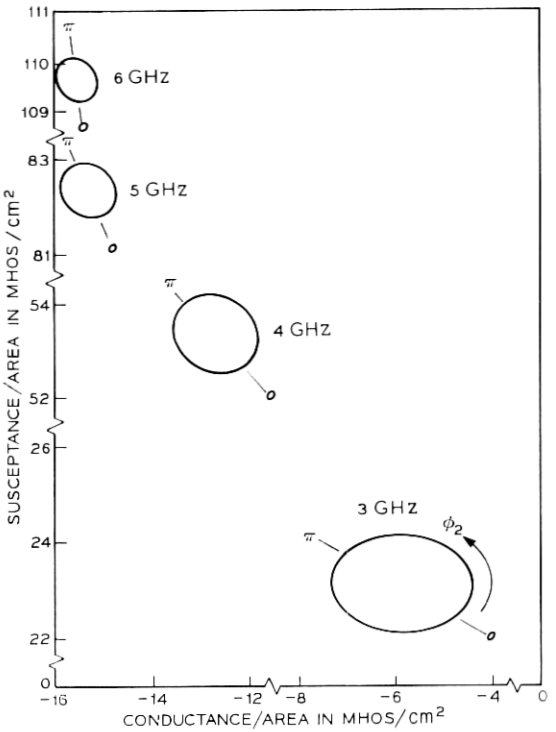

Fig. 3—The input admittance, Y_{in1}, at 3, 4, 5 and 6 GHz as it is modified by the presence of a second-harmonic voltage for $V_1 = 10$ volts, $V_2 = 1$ volt and $J_0 = 340$ A/cm².

$i_{21} = y_{21}V_1 \exp(j\varphi_1)$. Selecting the lowest-order terms having the appropriate frequencies, we find that

$$y_{12} \propto V_1 \exp(-j\varphi_1)$$

and (3)

$$y_{21} \propto V_1 \exp(j\varphi_1)$$

which confirms the approximate linear dependence on V_1 and gives the appropriate form of the φ_1 dependence. It will be convenient later to approximate y_{12} and y_{21} by the quantities

$$\begin{aligned} \bar{y}_{12} &= K_1 V_1 \exp(-j\varphi_1) = \kappa_1 V_1 \exp[-j(\varphi_1 - \psi_1)], \\ \bar{y}_{21} &= K_2 V_1 \exp(j\varphi_1) = \kappa_2 V_1 \exp[j(\varphi_1 + \psi_2)], \end{aligned} \tag{4}$$

where $\kappa_1 = |K_1|$, $\kappa_2 = |K_2|$, $\psi_1 = \arg(K_1)$ and $\psi_2 = \arg(K_2)$. Note that for $\varphi_1 = 0$ (only the phase $\varphi_2 - \varphi_1$ is important), $\psi_1 = \arg(y_{12})$ and $\psi_2 = \arg(y_{21})$ which is what will usually be assumed.

The quantities $\bar{y}_{12}$ and $\bar{y}_{21}$ may be defined as the average of y_{12} and y_{21} over the phase φ_2. For the 6-GHz oscillator example, the calculated values of $\bar{y}_{12}$ and $\bar{y}_{21}$ as a function of frequency are shown in Figs. 7 and 8 and the phases ψ_1, ψ_2 and $\psi_1 + \psi_2$ are shown in Fig. 9. Obviously these are only first-order approximations, but the complexity of the stability analysis requires some suitable approximation to obtain qualitative understanding.

The interaction of the diode equivalent circuit of Fig. 1 with an external circuit can be visualized by connecting an admittance Y_2 to the second-harmonic port. The fundamental input admittance is then

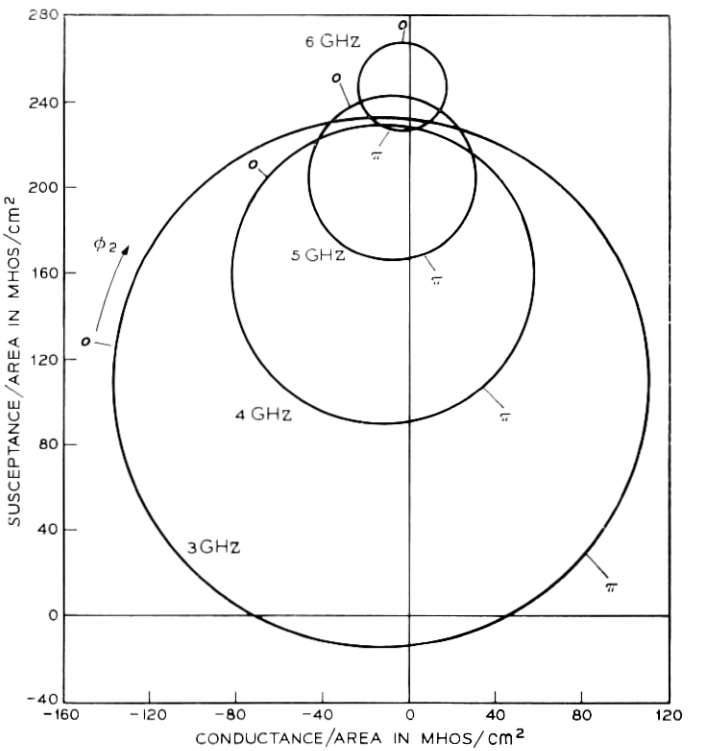

Fig. 4—The input admittance, Y_{in2}, at the second harmonic of 3, 4, 5 and 6 GHz for the same conditions as Fig. 3.

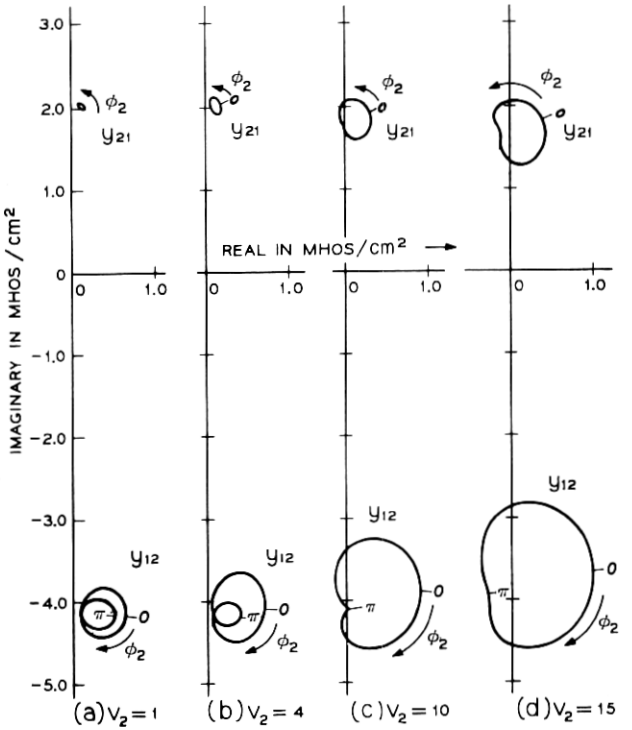

Fig. 5—Complex plane plot of y_{12} and y_{21} for $V_1 = 10$ volts and $V_2 = 2, 6, 10, 14$ volts at 6 GHz, showing the relative insensitivity of y_{12} and y_{21} to changes in V_2 and φ_2 for moderate values of V_2.

$$Y_{in1} = y_{11} - \frac{y_{12}y_{21}}{y_{22} + Y_2}. \tag{5}$$

Tuning the second harmonic by adjusting Y_2 provides the possibility of almost any input admittance Y_{in1}. In particular, $| Y_2 | = \infty$ gives the short-circuit termination and $Y_{in1} = y_{11}$. Equation (5) also predicts a pole in Y_{in1} at the frequency for which $y_{22} + Y_2 = 0$. This is not an ordinary pole as in linear circuit theory however for two reasons: (*i*) y_{22} may have a negative real part because it is an active device, and (*ii*) y_{22} is a function of V_2 so that the "pole" at $y_{22} + Y_2 = 0$ moves with changing V_2. This means that a resonance type of behavior should be observed, but that the only condition where $y_{22} + Y_2 = 0$ is for $V_1 \equiv 0$, which is just the single-frequency oscillator condition at $2f$.

III. STABILITY OF THE OSCILLATION STATE

Given an oscillation state which prescribes the admittances at the two frequencies, there are two requirements on the circuit that must be met in order that this be an obtainable state of steady oscillations. These are the requirements of circuit realizability and oscillation-state stability. The realizability criterion is simply that the required circuit have admittances whose real parts are greater than zero. The stability criterion is that any perturbation away from the given state will asymptotically return to the original state.

The stability problem has been recently discussed by Kurokawa[9,10] for the single-frequency negative-resistance oscillator. By following the approach used by Kurokawa and extending it to two-frequency interactions, the equations governing the stability of the harmonically tuned oscillator are derived in Appendix A. In this section, they are

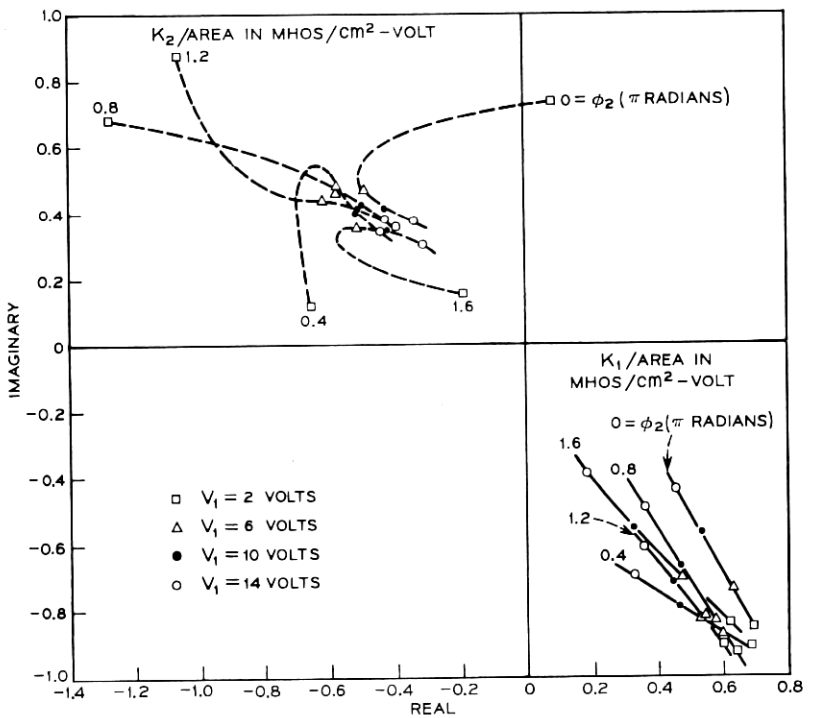

Fig. 6—Complex plane plot of $K_1 = y_{12}/V_1$ and $K_2 = y_{21}/V_1$ as a function of V_1 for various values of second-harmonic phase φ_2, at 4 GHz.

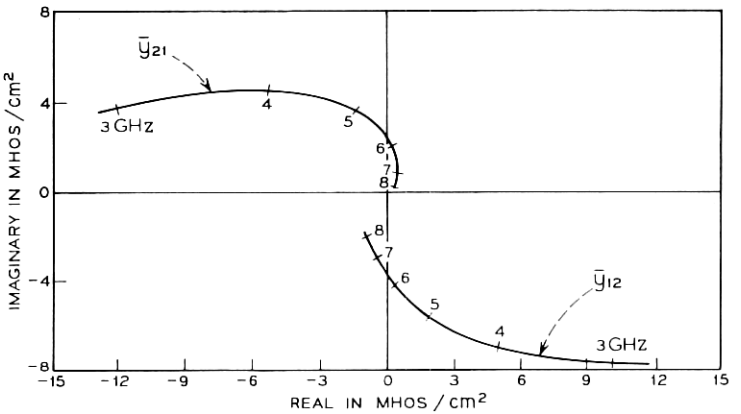

Fig. 7—Complex plane plot of $\bar{y}_{12}$ and $\bar{y}_{21}$ as a function of the fundamental frequency for $V_1 = 10$ volts and $V_2 = 1$ volt.

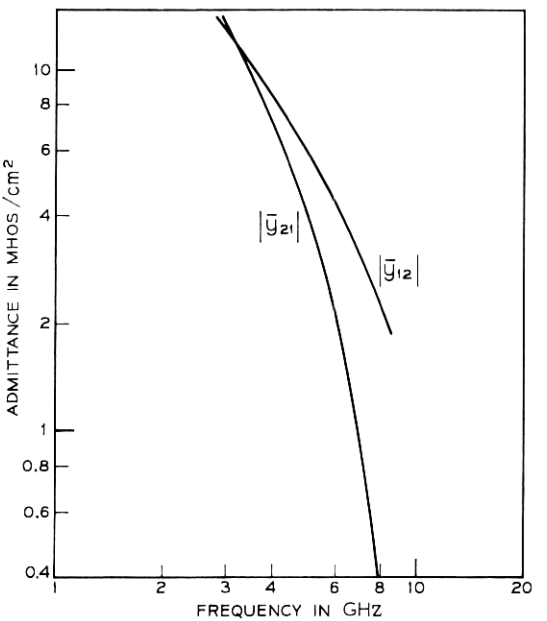

Fig. 8—$|\bar{y}_{12}|$ and $|\bar{y}_{21}|$ versus frequency for $V_1 = 10$ volts and $V_2 = 1$ volt.

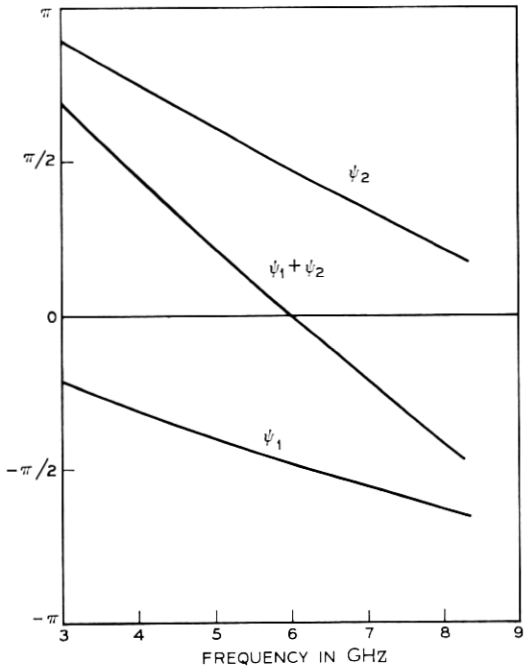

Fig. 9—The arguments ψ_1, ψ_2 and $\psi_1 + \psi_2$ versus frequency, showing a nearly linear dependence.

applied to several special cases, and theoretical examples of their use with the 6-GHz germanium oscillator model of Blue are given in Section IV.

In Appendix A, it is shown that the stability of an oscillation-state for small perturbations is determined by the solution of the system of equations

$$\frac{d\epsilon}{dt} + B\epsilon = 0 \tag{6}$$

where the vector ϵ is defined as

$$\epsilon = \begin{pmatrix} \delta a_1/V_1 \\ \delta a_2/V_2 \\ \delta(\varphi_2 - 2\varphi_1) \end{pmatrix} \tag{7}$$

and the matrix B is given by

$$B = \begin{bmatrix} \dfrac{\sqrt{r^2+s^2}\,G_{10}}{|Y_1'|}\sin(\alpha_1-\gamma_1) & \dfrac{\kappa_1 V_2}{|Y_1'|}\sin(\alpha_1+\theta_{10}) & -\dfrac{\kappa_1 V_2}{|Y_1'|}\cos(\alpha_1+\theta_{10}) \\ \dfrac{\kappa_2 V_1}{|Y_2'|}\sin(\alpha_2+\theta_{20}) & \dfrac{\sqrt{u^2+v^2}\,G_{20}}{|Y_2'|}\sin(\alpha_2-\gamma_2) & \dfrac{\kappa_2 V_1}{|Y_2'|}\cos(\alpha_2+\theta_{20}) \\ \left\{\dfrac{-2\sqrt{r^2+s^2}\,G_{10}}{|Y_1'|}\cos(\alpha_1-\gamma_1)\right\} & \left\{\dfrac{\sqrt{u^2+v^2}\,G_{20}}{|Y_2'|}\cos(\alpha_2-\gamma_2)\right\} & \left\{-\dfrac{2\kappa_1 V_2}{|Y_1'|}\sin(\alpha_1+\theta_{10})\right\} \\ \left\{+\dfrac{\kappa_2 V_1}{|Y_2'|}\cos(\alpha_2+\theta_{20})\right\} & \left\{-\dfrac{2\kappa_1 V_2}{|Y_1'|}\cos(\alpha_1+\theta_{10})\right\} & \left\{-\dfrac{\kappa_2 V_1}{|Y_2'|}\sin(\alpha_2+\theta_{20})\right\} \end{bmatrix}. \tag{8}$$

As discussed in the Appendix, δa_1, δa_2 and $\delta(\varphi_2 - 2\varphi_1)$ are the perturbations in the fundamental and second-harmonic voltage amplitudes and the relative phase, respectively. V_1 and V_2 are the unperturbed values of fundamental and second-harmonic voltage amplitudes.

The remaining quantities in the B matrix are defined as follows. The fundamental and second-harmonic external circuit admittances are $Y_1(\omega_0) = G_{10} + jB_{10}$ and $Y_2(2\omega_0) = G_{20} + jB_{20}$, respectively. The primes on Y_1 and Y_2 in equation (8) denote differentiation with respect to frequency at ω_0 and $2\omega_0$ respectively. κ_1 and κ_2 are defined in equation (4).

The saturation parameters s, r and u, v are defined by equations (55) through (58) in the Appendix. They relate to the nonlinear saturation of the diode's conductance and susceptance at the fundamental and second harmonic frequencies, respectively. The significance of s and r is shown schematically in Fig. 10, with u and v interpreted by a similar diagram for the second-harmonic admittance.

We have also introduced the angles α_1 and α_2 which give the slope on the complex plane of the circuit admittances at ω_0 and $2\omega_0$

$$\cos \alpha_1 = \frac{G'_{10}}{\sqrt{G'^2_{10} + B'^2_{10}}}, \qquad \sin \alpha_1 = \frac{B'_{10}}{\sqrt{G'^2_{10} + B'^2_{10}}} \tag{9}$$

$$\cos \alpha_2 = \frac{G'_{20}}{\sqrt{G'^2_{20} + B'^2_{20}}}, \qquad \sin \alpha_2 = \frac{B'_{20}}{\sqrt{G'^2_{20} + B'^2_{20}}} \tag{10}$$

and the angles γ_1 and γ_2 which measure the slope of the admittance curves $y_{11}(V_1)$ and $y_{22}(V_2)$;

$$\cos \gamma_1 = \frac{s}{\sqrt{r^2 + s^2}}, \qquad \sin \gamma_1 = \frac{r}{\sqrt{r^2 + s^2}}; \tag{11}$$

$$\cos \gamma_2 = \frac{u}{\sqrt{u^2 + v^2}}, \qquad \sin \gamma_2 = \frac{v}{\sqrt{u^2 + v^2}}. \tag{12}$$

Also, θ_{10} and θ_{20} are defined as in equations (48) and (49) of the Appendix but with the phase φ_1 set to zero. That is

$$\theta_{10} = -\varphi_2 - \psi_1$$

and (13)

$$\theta_{20} = \varphi_2 - \psi_2.$$

Note that

$$\theta_{10} + \theta_{20} = -\psi_1 - \psi_2. \tag{14}$$

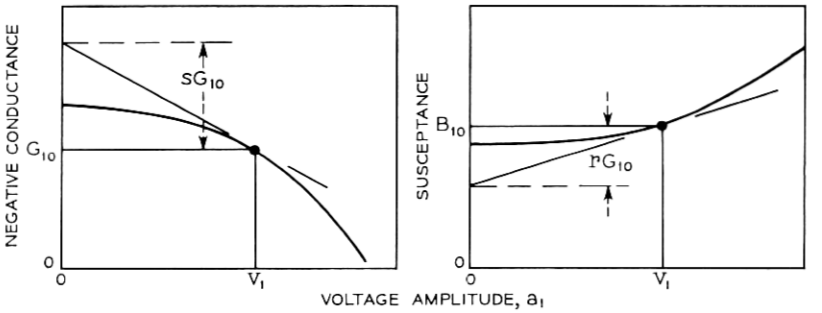

Fig. 10—Interpretation of the saturation parameters s and r for the fundamental admittance y_{11}. Similar definitions hold for u and v for the second-harmonic admittance y_{22}.

For the Ge oscillator considered here, the direct relationship between φ_2, θ_{20} and θ_{10}, as determined from equation (13), is shown in Fig. 11 for several frequencies.

The angles α_1, γ_1 and θ_{10} are shown in Fig. 12 which is a plot of the negative of an assumed circuit admittance $-Y_1(\omega)$ and the diode single-frequency admittance $y_{11}(V_1)$ in the neighborhood of the fundamental frequency. The point of intersection at ω_s gives the frequency and amplitude of the fundamental oscillation with zero second-harmonic voltage. As the voltage V_2 is increased by presenting an appropriate value of $Y_2(2\omega_0)$, the frequency will shift to some new value ω_0 generally accompanied by a change in voltage to V_1. This shows that the current injected into the fundamental circuit by the $y_{12}V_2 \exp(j\varphi_2)$ current source of Fig. 1 is just that sufficient to obtain the difference between the admittances $-Y_1(\omega_0)$ and $y_{11}(V_1)$. This additional admittance may be considered as a vector pointing from $y_{11}(V_1)$ to $-Y_1(\omega_0)$, and it is the angle θ_{10} measured clockwise about the $y_{11}(V_1)$ point that determines the orientation of this vector. Its length is given by $|y_{12}|\ V_2/V_1$. The angle α_1 gives the slope of the circuit curve at $-Y_1(\omega_0)$, and the angle γ_1 gives the relative change in reactive to real part of $y_{11}(V_1)$ with increasing voltage V_1 at the operating point. The angles α_2, γ_2 and θ_{20} may be defined in a similar manner in the second-harmonic admittance plane.

The solution of equation (6) subject to a small initial perturbation has a decreasing amplitude with increasing time if the eigenvalues of the stability matrix B all have real parts greater than zero. Suitable tests have been devised to determine this property.[11] The general case is difficult to do analytically and generally difficult to interpret if done

numerically because of the large number of parameters of the system. This is done however for the 6-GHz oscillator example given in Section IV, and the results are compared with the simplified results of this section.

In the remainder of this section, three special cases are examined which are severe approximations to the general case, but which yield interesting information. The first of these is that of a single-frequency oscillator, $V_2 = 0$. The second is the fictitious weak-coupling case which does not apply to the germanium diodes modeled here, but is included because of simplicity and for completeness. The third case is that of a strongly coupled small-signal approximation which gives qualitatively most of the features observed from the complete study

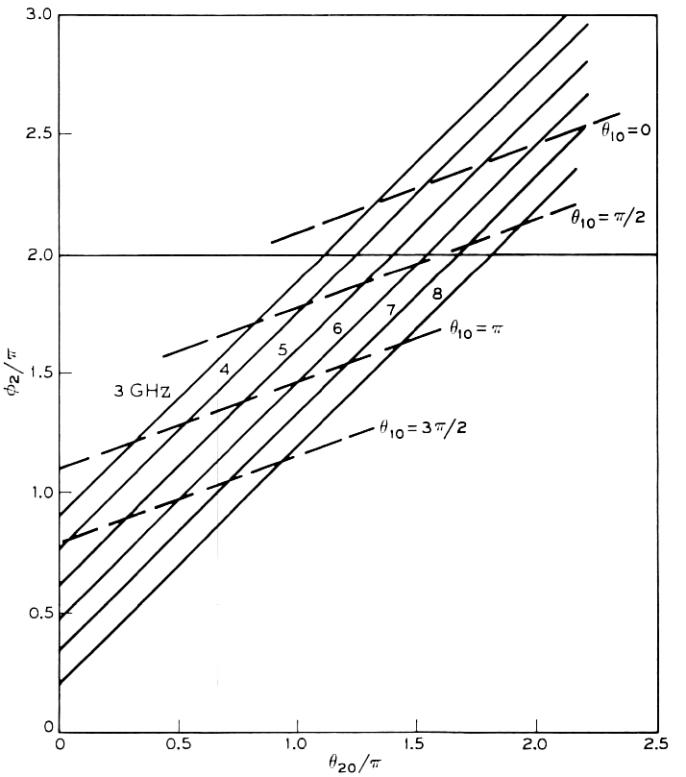

Fig. 11—Oscillator phase relations for the 6-GHz germanium example; φ_2 versus θ_{20} with loci of constant θ_{10} at 3, 4, 5, 6, 7 and 8 GHz.

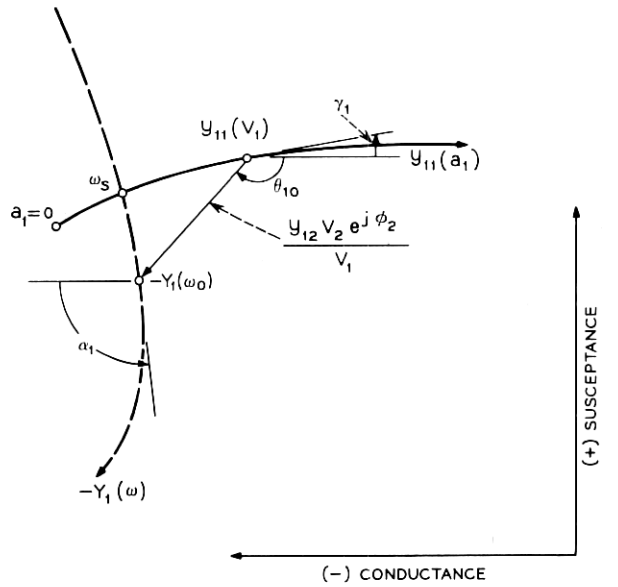

Fig. 12—An assumed fundamental admittance plane plot showing the angles α_1, γ_1 and θ_{10}. The device admittance is $y_{11}(a_1)$ and the negative of the circuit admittance is $-Y_1(\omega)$. A similar diagram defines α_2, γ_2 and θ_{20} in the neighborhood of $2\omega_0$.

of the eigenvalues of B, which is carried out in Section IV for the germanium diode case.

3.1 *Single-Frequency Limit*

In the very special case of $V_2 = 0$, only the first and third parts of equation (6) remain and they give the conditions

$$\sin(\alpha_1 - \gamma_1) > 0 \tag{15}$$

and

$$\frac{\kappa_2 V_1}{|Y_2'|} \sin(\alpha_2 + \theta_{20}) < 0. \tag{16}$$

These are simply the conditions required for stability of a single-frequency oscillator [equation (15)] with the added condition (16) due to the coupling to the harmonic. If the coupling to the harmonic, κ_2, is zero for $V_2 = 0$, equation (16) does not apply. Thus, for the single frequency oscillator with $V_2 = 0$, the familiar stability relation is recovered.[10]

3.2 *Weak-Coupling Limit*

For an oscillator having very small κ_1 and κ_2, the first two parts of equation (6) decouple. This gives

$$\sin(\alpha_j - \gamma_j) > 0 \qquad (j = 1, 2)$$

which are the single-frequency stability conditions at ω_0 and $2\omega_0$ for $j = 1$ and 2, respectively. The third equation then requires

$$\sin(\alpha_1 + \theta_{10}) + \mu \sin(\alpha_2 + \theta_{20}) < 0 \tag{17}$$

where the parameter μ is defined by

$$\mu = \frac{\kappa_2 V_1 \mid Y_1' \mid}{2\kappa_1 V_2 \mid Y_2' \mid}. \tag{18}$$

We may write equation (17) as

$$\sin(\varphi_2 + \xi) < 0 \tag{19}$$

where ξ is defined by the equations

$$\rho \sin \xi = -[\sin(\psi_1 - \alpha_1) + \mu \sin(\psi_2 - \alpha_2)] \tag{20}$$

and

$$\rho \cos \xi = -[\cos(\psi_1 - \alpha_1) - \mu \cos(\psi_2 - \alpha_2)]. \tag{21}$$

For a given pair of V_1, V_2 and for a fixed circuit, equation (19) thus gives the range of φ_2 for stable operation in the weak coupling limit.

3.3 *Small-Signal, Strong-Coupling Limit*

For very small signals the admittances y_{11} and y_{22} are independent of V_1 and V_2 so that $s \equiv r \equiv u \equiv v \equiv 0$ provides another approximation of some interest, providing that the coupling is still significant. In this limit, we obtain four constraints which are necessary and sufficient[11] to insure that the matrix B have positive eigenvalues. These are

$$k_1 = -\sin(\alpha_1 + \theta_{10}) - \mu \sin(\alpha_2 + \theta_{20}) > 0, \tag{22}$$

$$k_2 = -\sin(\alpha_1 + \theta_{10}) \cdot \sin(\alpha_2 + \theta_{20}) + 3 \cos(\alpha_1 + \theta_{10}) \cdot \cos(\alpha_2 + \theta_{20}) > 0, \tag{23}$$

$$k_3 = \sin(\alpha_2 + \theta_{20}) + \mu \sin(\alpha_1 + \theta_{10}) > 0, \tag{24}$$

$$k_4 = k_1 k_2 - k_3 > 0, \tag{25}$$

where μ is defined by equation (18).

The significance of this case is that for $\mu = 1$, conditions $k_1 > 0$ and $k_3 > 0$ are contradictory. This implies that $\mu = 1$ is a critical value and is indeed unstable, whereas for μ approaching zero or infinity stable states of oscillation do exist. These $\mu \ll 1$ and $\mu \gg 1$ stable states are exclusive of each other so that, as the conditions of oscillation are changed, if μ passes through the value unity a discontinuity in the oscillation will occur wherein the phase, the power and the frequency may all jump suddenly to new values.

To demonstrate the existence and exclusive nature of the $\mu \ll 1$ and $\mu \gg 1$ limits, consider equations (22) through (25) Note first of all that if a solution is obtained for a given value of μ, the solution for the reciprocal of that value of μ is obtained by interchanging the subscripts 1 and 2 on the angles α and θ. Thus, we need only consider the limit $\mu \ll 1$; the limit $\mu \gg 1$ being obtained from symmetry. For $\mu \ll 1$, equations (22) and (24) yield [Using equation (13)]

$$\pi - \psi_1 + \alpha_1 < \varphi_2 < 2\pi - \psi_1 + \alpha_1 \quad (k_1 > 0) \tag{26}$$

and

$$\psi_2 - \alpha_2 < \varphi_2 < \pi + \psi_2 - \alpha_2 \quad (k_3 > 0) \tag{27}$$

respectively. For purposes of illustration we consider $\alpha_1 = \alpha_2 = \bar{\alpha}$. Then the regions defined by equations (26) and (27) may be plotted in the φ_2, $\bar{\alpha}$ plane. From equation (25), if k_1, k_3 and k_4 are > 0, $k_2 > 0$ is automatically satisfied. Consider the constraint $k_4 > 0$, which may be written

$$-\cos(\alpha_1 + \theta_{10})[2 \sin(\alpha_1 + \theta_{10} + \alpha_2 + \theta_{20}) + \sin(\alpha_1 + \theta_{10} - \alpha_2 - \theta_{20})] > 0. \tag{28}$$

We see that $\cos(\alpha_1 + \theta_{10}) = 0$ is a critical condition, on either side of which the term in the brackets must also change sign. Thus, the lines

$$\varphi_2 = \psi_1 - \bar{\alpha} \pm \pi/2 \quad (k_4 = 0) \tag{29}$$

in the φ_2, $\bar{\alpha}$ plane are critical lines. Further, consider $\cos(\alpha_1 + \theta_{10}) > 0$, then

$$\sin(\psi_1 + \psi_2 - 2\bar{\alpha}) > -\sin(2\varphi_2 + \psi_1 - \psi_2)/2 \quad (k_4 > 0). \tag{30}$$

Equation (30) represents a curved boundary in the φ_2, $\bar{\alpha}$ plane and must be computed numerically. In Fig. 13 the regions bounded by equations (26), (27), (29) and (30) are plotted. The data used for this figure (ψ_1 and ψ_2) were taken from the Ge IMPATT example at a fre-

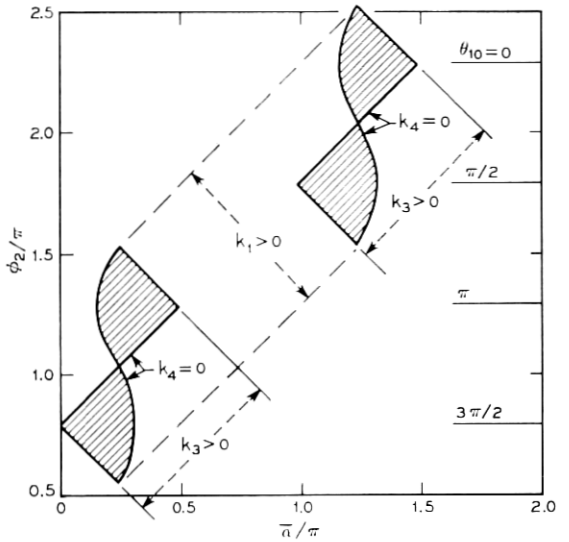

Fig. 13—Regions of stable φ_2 versus $\bar{\alpha}(\alpha_1 = \alpha_2 = \bar{\alpha})$ in the strongly coupled small-signal limit at 4 GHz; $\mu \ll 1$.

quency of 4 GHz from Fig. 9. Figure 13 shows that, for $\mu \ll 1$, there are two disjoint regions. Also indicated are the values of φ_2 for which $\theta_{10} = 0, \pi/2, \pi, 3\pi/2$. The angle θ_{10} (Fig. 12) measures the relative location of the diode's actual input conductance with respect to the single-frequency large-signal negative conductance, at the fundamental frequency. For $-\pi/2 < \theta_{10} < \pi/2$, $\cos \theta_{10}$ is positive and the input conductance is less negative than it would be for zero harmonic voltage. For this range of θ_{10} then, the fundamental output power is degraded by harmonic tuning. On the other hand, for $\pi/2 < \theta_{10} < 3\pi/2$, the input conductance is more negative than for $V_2 = 0$, and the fundamental output power is enhanced by the presence of harmonic tuning. These relationships can readily be seen by rewriting equation (1)

$$\mathrm{Re}\,(Y_{in1}) = -g_1 + |\,y_{12}\,|\,\frac{V_2 \cos \theta_{10}}{V_1}.$$

Indeed, $\theta_{10} = \pi$ maximizes the fundamental output power for the particular values of V_1, V_2 being studied. We see that at 4 GHz, the maximum fundamental power point exists within a stable region for $\mu \ll 1$. It is also interesting that the minimum fundamental power phase ($\theta_{10} = 0$) is in a separate region which requires a considerably different circuit.

To obtain the similar diagram for $\mu \gg 1$, the same considerations can be reapplied to k_1 through k_4, or the subscripts on φ and α can be interchanged. Either way, Fig. 14 shows the result. Comparison of Figs. 13 and 14 shows indeed the disjointed, mutually exclusive behavior of the $\mu \ll 1$ and $\mu \gg 1$ regions of stability. Additionally, it shows that for a given circuit (i.e., a given $\bar{\alpha}$), there are two stable ranges of phase φ_2 (if any at all) depending on the value of μ relative to unity. One of these encompasses the $\theta_{10} = \pi$ maximum power phase and the other encompasses the $\theta_{10} = 0$ minimum power phase. A change in the bias current, which does not alter significantly the circuit variable $\bar{\alpha}$, may well change the relative value of μ from >1 to <1 or vice versa, and such a change would necessitate a change of phase to a different branch. Thus, which branch of the stability diagram the oscillation state is in is determined by the history of tuning and bias current changes. This type of behavior would be observed experimentally as a hysteresis in frequency or power or both, which if analyzed would indicate that the input admittance of the diode at the fundamental frequency is a nonunique function of the fundamental RF voltage. The presence of this effect would be indicated if one were able to obtain two different values of power output for the same frequency

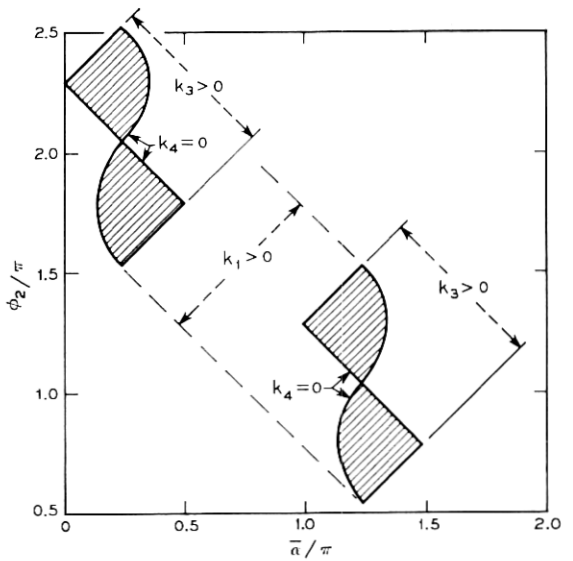

Fig. 14—Regions of stable φ_2 versus $\bar{\alpha}(\alpha_1 = \alpha_2 = \bar{\alpha})$ in the strongly coupled small-signal limit at 4 GHz; $\mu \gg 1$.

by changing the bias current only, without retuning the RF circuit in any respect. Observation at a single frequency is required in order to rule out the possibility of multiple-valued circuit admittances.[10]

In the next section, we compute the regions of stability for the germanium IMPATT example in full generality; that is, we use the complete form of the matrix B, equation (8). This must be done numerically so a limited number of cases can be examined, and the results are compared with the approximate forms of this section.

IV. 6-GHz Germanium Oscillator Example

Using Blue's approximate large-signal analysis,[1] the equivalent circuit parameters of Fig. 1 have been calculated for a germanium diode of depletion layer width 4.75 microns with an assumed avalanche zone width of 1.5 microns. This gives a critical field $E_c = 1.87 \times 10^5$ V/cm for a bias current density $J_0 = 340$ A/cm^2, which agrees quite well with the value obtained from a more exact numerical treatment. The design of this model was an attempt to model the germanium diodes reported by Swan[2] and by Gewartowski and Morris.[12] Because the Read theory is slightly incorrect in its reactive effects, the frequency of maximum negative conductance was at about 6 GHz for the model but appeared to be at about 8 or 9 GHz for the actual diodes. In comparing the results of this work with those of the experiments, it therefore seems most useful to discuss frequency relative to f_{max}, at which maximum output power is obtained. Thus, 4 GHz in this analytical work is roughly equivalent to 6 GHz in Swan's experiments. Table I lists the large-signal information obtained from Figs. 2, 8 and 9 that is needed for the solution of the stability constraints. This information was obtained for $V_1 = 10$ volts and $V_2 = 10$ volts, and a dc bias current density $J_0 = 340$ A/cm^2.

It is known that at resonance in a low-loss circuit where the real part of the admittance is constant or nearly so, the external Q can be written

$$Q_{ext} = \frac{\omega_0}{2G_0} \frac{dB}{d\omega} \bigg|_{\omega=\omega_0}$$

where G_0 is the real part of the admittance at ω_0 and B is the susceptance. Resonance is defined by the vanishing of $B(\omega_0)$. It is useful here to extend this definition to define the slope parameters

$$D_1 = \frac{\omega_0}{2G_{10}} \left| \frac{dY_1}{d\omega} \right|_{\omega=\omega_0}$$

TABLE I—DIODE LARGE-SIGNAL PARAMETERS AT $V_1 = V_2 = 10$ VOLTS

	3 GHz	4 GHz	5 GHz	6 GHz
g_{11} (mhos/cm²)	5.8	12.7	15.4	15.6
g_{22} (mhos/cm²)	15.6	12.7	8.5	4.3
$\frac{\partial g_1}{\partial V_1}$ (mhos/cm²-volt)	0.0	0.22	0.24	0.21
$\frac{\partial b_1}{\partial V_1}$ (mhos/cm²-volt)	1.1	0.65	0.30	0.20
$\frac{\partial g_2}{\partial V_2}$ (mhos/cm²-volt)	0.21	0.125	0.065	0.035
$\frac{\partial b_2}{\partial V_2}$ (mhos/cm²-volt)	0.20	0.0	0.0	0.0
ψ_1 (π radians)	−0.2089	−0.3056	−0.395	−0.477
ψ_2 (π radians)	0.9031	0.7742	0.6181	0.4798
κ_1 (mhos/cm²-volt)	1.25	0.86	0.59	0.42
κ_2 (mhos/cm²-volt)	1.25	0.70	0.385	0.205

at the fundamental frequency and

$$D_2 = \frac{\omega_0}{G_{20}} \left| \frac{dY_2}{d\omega} \right|_{\omega = 2\omega_0}$$

at the second harmonic. If, at $\omega = \omega_0$ and $\omega = 2\omega_0$, G'_{10} and G'_{20} vanish respectively, then D_1 and D_2 reduce to the external Q's of the circuit at these two frequencies, particularly since the major portion of the diode's susceptance is considered to be part of the external circuit.

Since, at an equilibrium point, from equations (44) and (46) of the Appendix

$$G_{10} = g_1 - \kappa_1 V_2 \cos \theta_1$$

and

$$G_{20} = g_2 - \kappa_2 V_1 \cos \theta_2 ,$$

specification of the parameters D_1 and D_2 permits the calculation of $| Y'_1 |$ and $| Y'_2 |$ from the information of Table I.

The general stability criteria for the matrix B are as follows: Let

B be represented

$$B = \begin{bmatrix} a & b & c \\ d & e & f \\ g & h & i \end{bmatrix}.$$

The condition that the eigenvalues of B all be positive implies that

$$k_1 = a + e + i > 0,$$

$$k_2 = ae + ei + ai - bd - fh - gc > 0,$$

$$k_3 = \det B > 0$$

and

$$k_4 = k_1 k_2 - k_3 > 0. \tag{31}$$

These conditions must be checked numerically, and the number of independent variables for a general study is quite large. In the calculations done here, the circuit variables have been restricted to $\alpha_1 = \alpha_2 = \bar{\alpha}$, with two sets of slope parameters; (*i*) $D_1 = 50$, $D_2 = 500$ and (*ii*) $D_1 = 50$, $D_2 = 10$. The restriction on α_1 and α_2 is quite artificial but allows comparison with the approximately determined regions of Section III. The two sets of slope parameters D_1, D_2 are an attempt to model (*i*) a high Q and (*ii*) a low Q second-harmonic circuit, respectively, and to thereby approximate the two conditions $\mu \ll 1$ and $\mu \gg 1$ for the same set of diode data.

The results of these calculations are shown in Figs. 15 and 16 for the frequencies 3, 4, 5 and 6 GHz. These show the values of stable second-harmonic phase φ_2 as functions of the circuit angles, $\alpha_1 = \alpha_2 = \bar{\alpha}$. These regions repeat themselves with a periodicity of 2π in both φ_2 and $\bar{\alpha}$. Only the principle branches are shown but it should be understood that wherever one of these regions extends across the boundaries chosen, it should be reflected back into the region at the opposite boundary. Figure 15 is for the case $D_1 = 50$, $D_2 = 500$, and corresponds to a value of $\mu \leq 0.4$ everywhere. Figure 16, for which $D_1 = 50$, $D_2 = 10$, corresponds to values of μ from near or slightly less than unity, to greater than 4 to 8 (the only exception is in Fig. 16a where one region appears having a value of $\mu \sim 0.02$). It should be noted that the value of $\mu \equiv 1$ is no longer a critical value, inasmuch as stable states may now exist for which $\mu = 1$. They do not appear to be large in number, however, and one may think of $\mu = 1$ as a transition value for which the area of the stable regions in the φ_2, $\bar{\alpha}$ plane becomes small.

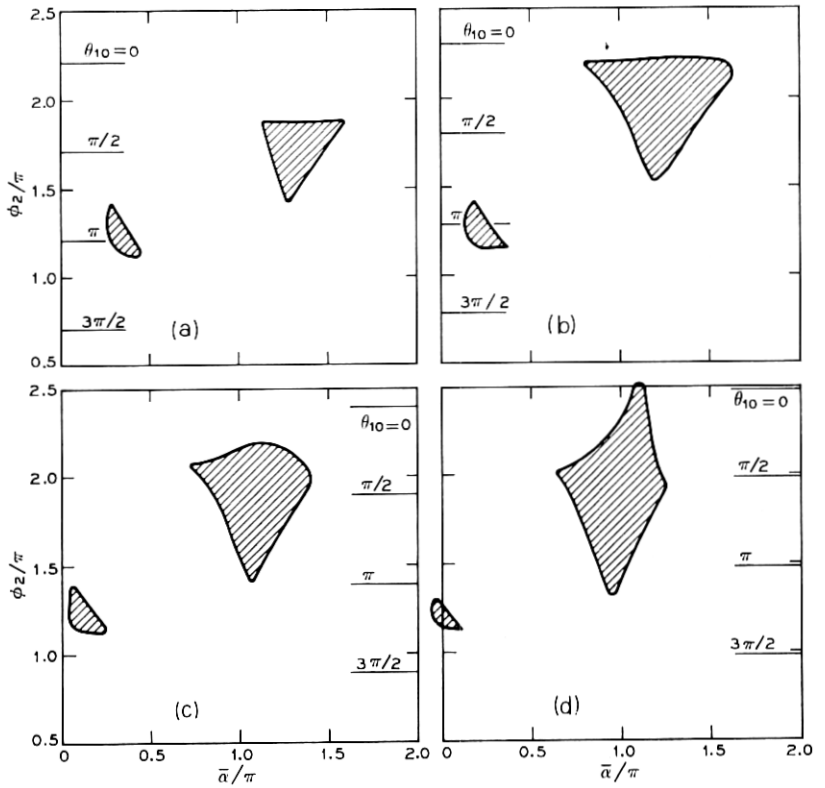

Fig. 15—Large-signal regions of stable φ_2 versus $\bar{\alpha}(\alpha_1 = \alpha_2 = \bar{\alpha})$ as obtained from the eigenvalues of the complete B matrix for the germanium oscillator example at (a) 3 GHz, (b) 4 GHz, (c) 5 GHz, and (d) 6 GHz; circuit variables $D_1 = 50$, $D_2 = 500$; diode variables $V_1 = V_2 = 10$ volts, $J_0 = 340$ A/cm^2. This figure has $\mu < 1$ everywhere.

Consider the 4-GHz results and compare Figs. 15b and 16b with Figs. 13 and 14. The locations of the stable regions in the φ_2, $\bar{\alpha}$ plane show a one-to-one correspondence but with greatly distorted shapes. It therefore appears that the strongly coupled small-signal approximation used in Figs. 13 and 14, together with the $\mu \ll 1$ and $\mu \gg 1$ cases, does give useful information about the general location of these stable regions for more realistic cases. The general properties of disjointedness and mutual exclusiveness are no longer strictly true (for example, there is some overlap of the regions centered at $\bar{\alpha} = \pi$ in Figs. 15d and 16d). However, it is easy to see that tuning discontinuities may still occur, and that the circuit angles $\bar{\alpha}$ must be considerably different

to obtain oscillation at $\theta_{10} = \pi$, for example, for the two different sets of values of slope parameters considered.

It is interesting that the angles α_1 and α_2 (and therefore, $\bar{\alpha}$) are equal to $\pi/2$ for simple shunt resonant circuits at both ω and 2ω, and that the stability diagrams show no cases of stable operation for this condition. Because of the approximations of this analysis, this cannot be construed to be a general conclusion, even for the diode modeled. It does show however, that such conditions may arise and that obtaining just the correct phase relations for maximum output power with a given circuit may be extremely difficult.

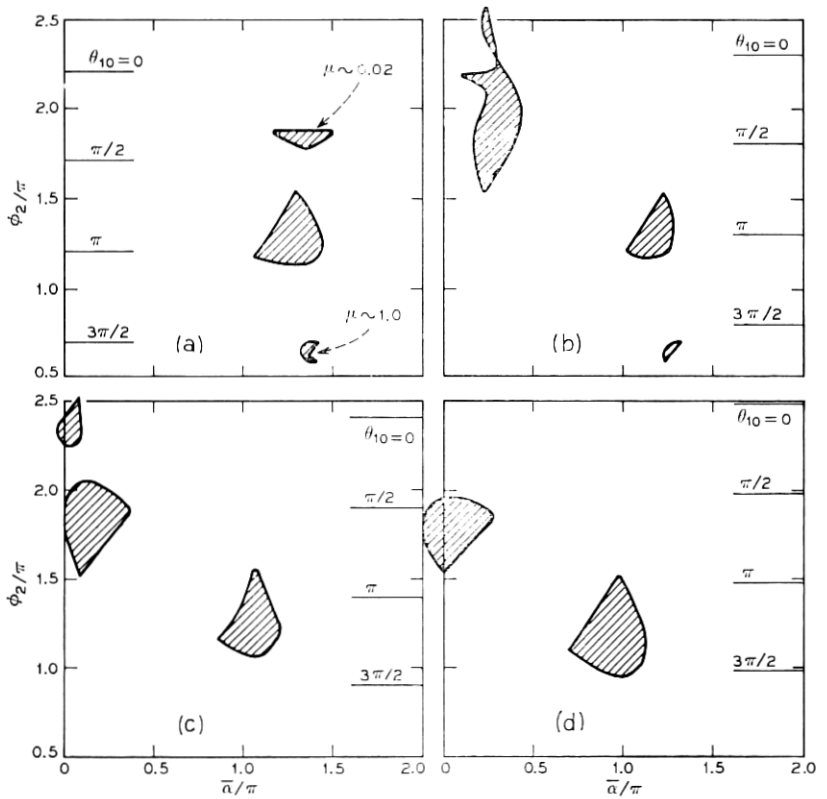

Fig. 16—Large-signal regions of stable φ_2 versus $\bar{\alpha}(\alpha_1 = \alpha_2 = \bar{\alpha})$ as obtained from the eigenvalues of the complete B matrix for the germanium oscillator example at (a) 3 GHz, (b) 4 GHz, (c) 5 GHz, and (d) 6 GHz; circuit variables $D_1 = 50$, $D_2 = 10$; diode variables $V_1 = V_2 = 10$ volts, $J_0 = 340$ A/cm^2. This figure has $\mu > 1$ everywhere except as noted.

Another observation is that the angle $\theta_{10} = \pi$ for maximum fundamental power output does have a stable realization in almost every case examined, even with the restriction $\alpha_1 = \alpha_2$.

If the points of operation along the circuit admittance curves $Y_1(\omega_0)$, $Y_2(2\omega_0)$ are near minima of their real parts, the angles α_1 and α_2 are restricted to lie in the range $0 < \alpha_j < \pi$, $j = 1, 2$. Such a limitation seems to imply different possibilities at the four frequencies calculated. At 3 GHz, stability is obtained in the neighborhood of $\theta_{10} = \pi$ and only for the $D_2 = 500$ case ($\mu < 1$). At 4 GHz, stability near $\theta_{10} = \pi$ is only obtained for the $D_2 = 500$ ($\mu < 1$) case, but there are additional stable states at or near $\theta_{10} = 0$ for both the $D_2 = 500$ ($\mu < 1$) and $D_2 = 10$ ($\mu > 1$) cases. Also, at 4 GHz, Fig. 16b shows a region which encompasses the $\theta_{10} = \pi/2$ point which is a crossover between enhanced and degraded fundamental power. The 5-GHz cases are very similar to those at 4 GHz except that there are more enhanced-power stable states for the $D_2 = 10$ ($\mu > 1$) case than at the lower frequencies. At 6 GHz, this shift is more advanced with roughly an equal number of stable states in the enhanced power region for the $D_2 = 10$ ($\mu > 1$) and $D_2 = 500$($\mu < 1$) cases.

V. SUMMARY AND CONCLUSIONS

An analysis of the stability of the tuned-harmonic mode in IMPATT oscillators has been presented using a simplified model of the frequency conversion in the avalanche diode. It has been shown that the stability constraints are generally quite restrictive and difficult to satisfy, particularly for diodes showing strong harmonic interactions. The goal of this work has not been to present a set of design curves which insure stable tuned-harmonic operation, but rather to consider the difficulties which the stability constraints present.

When the circuit restricts the voltage across the diode to be largely sinusoidal, this analysis reduces to that of the stability of a "single-frequency" oscillator. For nonzero fundamental and second-harmonic voltages V_1 and V_2, a characteristic parameter μ has been defined [equation (18)] which is dependent upon both diode and circuit characteristics and degree of excitation. The value of $\mu = 1$ appears to be somewhat critical in that the stable regions for $\mu > 1$ and $\mu < 1$ are usually separate. Any tuning or bias changes which force μ to pass through unity are very likely to produce sudden changes in the output variables, i.e., power and frequency. For example, the single-frequency oscillator is destined to have $\mu \gg 1$ because of the small value of V_2.

However, for equal V_1 and V_2 and $D_2/D_1 \sim 10$, $\mu < 0.4$. Thus the single-frequency oscillator and the tuned-harmonic oscillator (high Q, $2\omega_0$ circuit) are likely to operate in different regions of stability.

The numerical treatment of the stability criteria have been restricted to the case where the circuit angles α_1 and α_2 are equal. Thus the results presented here cannot be considered complete. However, in the example studied, it was found that at an operating frequency two-thirds the frequency of maximum output power, the phase φ_2 for maximum power is indeed stable and also corresponds to a realizable circuit. It was also found that it is possible to degrade the output power, and therefore, harmonic interactions when improperly adjusted can severely lower a diode's output power from that which would exist with no harmonic voltage at all.

As a necessary part of this instability analysis, a two-port model for the interaction was introduced and characterized for the 6-GHz germanium IMPATT model presented. This characterization illustrates the role of the second harmonic in introducing a "pseudo-pole" into the nonlinear admittance of the fundamental, and it clarifies the relevance of the single-frequency admittance plane characterization for the tuned-harmonic mode of operation.

This analysis also has assumed that y_{12} and y_{21} may be described by equation (4). If, on the other hand, y_{12} and y_{21} are assumed constant, then this analysis becomes identical with that of two nonlinear oscillators coupled through a linear circuit. That analysis can be carried through in the same manner as presented here. In such a case, the weakly coupled case becomes of considerable interest and has been treated by Schlosser.[13]

It is not necessary, of course, to introduce the two-port model of Fig. 1 at all, with its attendant assumptions and approximations, but it is possible to consider the perturbation of the oscillation-state directly from the numerical solution of the IMPATT equations. This would be a more accurate method to pursue; however, it is felt that the approach presented in this paper provides insight that might be obscured in a more complicated approach.

VI. ACKNOWLEDGMENTS

The author would like to acknowledge many helpful discussions with J. W. Gewartowski and K. Kurokawa in the development of this work, and the use of the approximate large-signal analysis computer program originally written by J. L. Blue.

APPENDIX A

Derivation of the Stability Matrix

In this appendix, the stability of the oscillation-state is considered using a linearized perturbation treatment about any general large-signal operating state. The result of this appendix is the derivation of the state-equation (6) and the stability matrix B, equation (8).

Consider a prescribed state of oscillation satisfying the two conditions

$$Y_1(\omega_0) + Y_{in1}(V_1 , V_2 , \varphi_1 , \varphi_2) = 0 \tag{32}$$

and

$$Y_2(2\omega_0) + Y_{in2}(V_1 , V_2 , \varphi_1 , \varphi_2) = 0, \tag{33}$$

where $Y_1(\omega_0)$ and $Y_2(2\omega_0)$ are the circuit admittances at ω_0 and $2\omega_0$ respectively. An approximation is made that the input admittances of the diode, Y_{in1} and Y_{in2}, are slowly varying functions of frequency as compared with the circuit admittances $Y_1(\omega_0)$ and $Y_2(2\omega_0)$. This is facilitated by considering the depletion layer capacitance, for example, to be a part of the external circuit. Generally speaking, equations (32) and (33) prescribe a functional dependence of ω, the frequency of oscillation, upon the voltage amplitudes and phases for small variations. For small variations in ω we can approximate

$$Y_1(\omega_0 + \delta_1) \approx Y_1(\omega_0) + \frac{dY_1}{d\omega}\bigg|_{\omega_0} \cdot \delta_1$$

and

$$Y_2(2\omega_0 + \delta_2) \approx Y_2(2\omega_0) + \frac{dY_2}{d\omega}\bigg|_{2\omega_0} \cdot \delta_2 .$$

The δ_k can be determined by allowing the voltage amplitudes and phases to be slowly varying functions of time

$$v_1(t) = a_1(t) \cos [\omega_0 t + \varphi_1(t)] \tag{34}$$

and

$$v_2(t) = a_2(t) \cos [2\omega_0 t + \varphi_2(t)]. \tag{35}$$

Differentiating with respect to time gives

$$\frac{dv_1}{dt} = \text{Re}\left\{\left[j\omega_0 + j\frac{d\varphi_1}{dt} + \frac{1}{a_1}\frac{da_1}{dt}\right]a_1 \exp [j(\omega_0 t + \varphi_1)]\right\} \tag{36}$$

and

$$\frac{dv_2}{dt} = \mathrm{Re}\left\{\left[2j\omega_0 + j\frac{d\varphi_2}{dt} + \frac{1}{a_2}\frac{da_2}{dt}\right]a_2 \exp\left[j(2\omega_0 t + \varphi_2)\right]\right\}. \tag{37}$$

Thus, we can identify[10]

$$\delta_1 = \frac{d\varphi_1}{dt} - j\frac{1}{a_1}\frac{da_1}{dt}$$

and

$$\delta_2 = \frac{d\varphi_2}{dt} - j\frac{1}{a_2}\frac{da_2}{dt},$$

and therefore

$$Y_1(\omega_0 + \delta_1) \approx Y_1(\omega_0) + \frac{dY_1}{d\omega}\bigg|_{\omega_0} \cdot \left(\frac{d\varphi_1}{dt} - j\frac{1}{a_1}\frac{da_1}{dt}\right) \tag{38}$$

and

$$Y_2(2\omega_0 + \delta_2) \approx Y_2(2\omega_0) + \frac{dY_2}{d\omega}\bigg|_{2\omega_0} \cdot \left(\frac{d\varphi_2}{dt} - j\frac{1}{a_2}\frac{da_2}{dt}\right) \tag{39}$$

are the circuit admittances related to slow variations of the amplitudes and phases.

From the equivalent circuit of Fig. 1, the currents at the fundamental and second harmonic are

$$i_1(t) = \mathrm{Re}\left\{[y_{11}a_1 \exp(j\varphi_1) + y_{12}a_2 \exp(j\varphi_2)] \cdot \exp(j\omega_0 t)\right\}$$

and

$$i_2(t) = \mathrm{Re}\left\{[y_{21}a_1 \exp(j\varphi_1) + y_{22}a_2 \exp(j\varphi_2)] \cdot \exp(j2\omega_0 t)\right\},$$

which may be rewritten using the assumptions (4) as

$$\begin{aligned} i_1(t) = {} & [-g_1 a_1 + \kappa_1 a_1 a_2 \cos(2\varphi_1 - \varphi_2 - \psi_1)] \cos(\omega_0 t + \varphi_1) \\ & + [-b_1 a_1 + \kappa_1 a_1 a_2 \sin(2\varphi_1 - \varphi_2 - \psi_1)] \sin(\omega_0 t + \varphi_1) \end{aligned} \tag{40}$$

and

$$\begin{aligned} i_2(t) = {} & [-g_2 a_2 + \kappa_2 a_1^2 \cos(\varphi_2 - 2\varphi_1 - \psi_2)] \cos(2\omega_0 t + \varphi_2) \\ & + [-b_2 a_2 + \kappa_2 a_1^2 \sin(\varphi_2 - 2\varphi_1 - \psi_2)] \sin(2\omega_0 t + \varphi_2). \end{aligned} \tag{41}$$

Here we have introduced

$$y_{11} = -g_1 + jb_1$$

and

$$y_{22} = -g_2 + jb_2 .$$

Kirchoff's laws for the nonequilibrium case are

$$i_1(t) + \text{Re}\,\{Y_1(\omega_1)a_1 \exp(j\varphi_1) \exp(j\omega_0 t)\} = 0 \tag{42}$$

and

$$i_2(t) + \text{Re}\,\{Y_2(\omega_2)a_2 \exp(j\varphi_2) \exp(j2\omega_0 t)\} = 0, \tag{43}$$

where ω_1 and ω_2 are the perturbed fundamental and second-harmonic frequencies.

Equations (40) and (41) with (42) and (43) give the following four differential equations for the quantities $a_1(t)$, $a_2(t)$, $\varphi_1(t)$ and $\varphi_2(t)$

$$G_1 - g_1 + G_1' \frac{d\varphi_1}{dt} + B_1' \frac{1}{a_1}\frac{da_1}{dt} = -\kappa_1 a_2 \cos\theta_1 , \tag{44}$$

$$-(B_1 + b_1) - B_1' \frac{d\varphi_1}{dt} + G_1' \frac{1}{a_1}\frac{da_1}{dt} = -\kappa_1 a_2 \sin\theta_1 , \tag{45}$$

$$G_2 - g_2 + G_2' \frac{d\varphi_2}{dt} + B_2' \frac{1}{a_2}\frac{da_2}{dt} = -\kappa_2 a_1 \cos\theta_2 , \tag{46}$$

$$-(B_2 + b_2) - B_2' \frac{d\varphi_2}{dt} + G_2' \frac{1}{a_2}\frac{da_2}{dt} = -\kappa_2 a_1 \sin\theta_2 . \tag{47}$$

Here we have defined $Y_1 = G_1 + jB_1$, $Y_2 = G_2 + jB_2$ and the primes denote differentiation with respect to ω. Also

$$\theta_1 = 2\varphi_1 - \varphi_2 - \psi_1 \tag{48}$$

and

$$\theta_2 = \varphi_2 - 2\varphi_1 - \psi_2 . \tag{49}$$

Equations (44) through (47) may be rewritten so as to contain only a single time derivative in each

$$B_1'(G_1 - g_1) - G_1'(B_1 + b_1) + |Y_1'|^2 \frac{1}{a_1}\frac{da_1}{dt} = -\kappa_1 a_2 [B_1' \cos\theta_1 + G_1' \sin\theta_1], \tag{50}$$

$$G_1'(G_1 - g_1) + B_1'(B_1 + b_1) + |Y_1'|^2 \frac{d\varphi_1}{dt} = -\kappa_1 a_2 [G_1' \cos\theta_1 - B_1' \sin\theta_1], \tag{51}$$

$$B_2'(G_2 - g_2) - G_2'(B_2 + b_2) + |\, Y_2' \,|^2 \frac{1}{a_2}\frac{da_2}{dt} = -\kappa_2 a_1[B_2' \cos\theta_2 + G_2' \sin\theta_2], \tag{52}$$

$$G_2'(G_2 - g_2) + B_2'(B_2 + b_2) + |\, Y_2' \,|^2 \frac{d\varphi_2}{dt} = -\kappa_2 a_1[G_2' \cos\theta_2 - B_2' \sin\theta_2]. \tag{53}$$

Since φ_1 is an aribitrary quantity with no physical significance, it can be eliminated in favor of the difference phase $\varphi_2 - 2\varphi_1$ since this appears in both θ_1 and θ_2. This is done by multiplying equation (51) by $2/|\, Y_1' \,|^2$, equation (53) by $1/|\, Y_2' \,|^2$ and subtracting equation (51) from (53), giving

$$\frac{d}{dt}(\varphi_2 - 2\varphi_1) + \frac{G_2'(G_2 - g_2) + B_2'(B_2 + b_2)}{|\, Y_2' \,|^2} - 2\,\frac{G_1'(G_1 - g_1) + B_1'(B_1 + b_1)}{|\, Y_1' \,|^2} = -\kappa_2 a_1\left(\frac{G_2' \cos\theta_2 - B_2' \sin\theta_2}{|\, Y_2' \,|^2}\right) + 2\kappa_1 a_2\left(\frac{G_1' \cos\theta_1 - B_1' \sin\theta_1}{|\, Y_1' \,|^2}\right). \tag{54}$$

Equations (50), (52) and (54) form the set of differential equations for $a_1(t)$, $a_2(t)$ and $\varphi_2(t) - 2\varphi_1(t)$ which will be linearized for small perturbations around the oscillation state. These perturbations take the form

$$a_1 = V_1 + \delta a_1 ,$$

$$a_2 = V_2 + \delta a_2 ,$$

and

$$\varphi_2 - 2\varphi_1 = \varphi_{20} - 2\varphi_{10} + \delta(\varphi_2 - 2\varphi_1),$$

where V_1, V_2, φ_{10} and φ_{20} are the unperturbed values of $a_1(t)$, $a_2(t)$, $\varphi_1(t)$ and $\varphi_2(t)$. The perturbations in the voltage amplitudes will change g_1, b_1, g_2, b_2 away from their values $\bar{g}_1$, $\bar{b}_1$, $\bar{g}_2$, $\bar{b}_2$ which correspond to $\delta a_1 = \delta a_2 = \delta(\varphi_2 - 2\varphi_1) \equiv 0$. Thus, we define the saturation parameters s, r, u, v which describe the linearized variation of g_1 around $\bar{g}_1$, etc., by the equations (see Fig. 10)

$$s = \frac{V_1}{G_{10}}\frac{\delta(G_{10} - g_1)}{\delta a_1} , \tag{55}$$

$$r = \frac{V_1}{G_{10}} \frac{\delta(B_{10} + b_1)}{\delta a_1} , \tag{56}$$

$$u = \frac{V_2}{G_{20}} \frac{\delta(G_{20} - g_2)}{\delta a_2} , \tag{57}$$

and

$$v = \frac{V_2}{G_{20}} \frac{\delta(B_{20} + b_2)}{\delta a_2} , \tag{58}$$

where the zero subscript on the circuit variables denotes their evaluation at ω_0 or $2\omega_0$ as appropriate.

Equations (50), (52) and (54) may now be cast in a simple matrix form

$$\frac{d\epsilon}{dt} + B\epsilon = 0 \tag{59}$$

where the vector ϵ is defined as

$$\epsilon = \begin{bmatrix} \delta a_1/V_1 \\ \delta a_2/V_2 \\ \delta(\varphi_2 - 2\varphi_1) \end{bmatrix} \tag{60}$$

and the matrix B is given by equation (8) of Section III. Equation (59) indicates that the perturbations decay with time, giving a stable state of oscillation, if the eigenvalues of the matrix B are all positive.

APPENDIX B

List of Symbols

a_1 , a_2	Slowly varying amplitudes of the fundamental and second-harmonic voltages; equations (34) and (35).
B	Stability matrix; equation (8).
B_1 , B_2	Fundamental and second-harmonic external circuit susceptances; following equation (47).
b_1 , b_2	Imaginary parts of y_{11} and y_{22}, the susceptances of the single-frequency oscillator admittances; following equation (41).
D_1 , D_2	Fundamental and second-harmonic external circuit slope parameters; Section IV.
G_1 , G_2	Fundamental and second-harmonic external circuit conductances; following equation (47).

g_1 , g_2 Negative of the conductances of the single-frequency oscillator admittances; following equation (41).

K_1 , K_2 Complex normalized form of y_{12} and y_{21}; equation (4).

s, r Saturation parameters for the admittance y_{11}; equations (55) and (56).

u, v Saturation parameters for the admittance y_{22}; equations (57) and (58).

V_1 , V_2 Fundamental and second-harmonic voltage amplitudes; preceding equation (1).

Y_1 , Y_2 Fundamental and second-harmonic external circuit admittances; Fig. 1.

Y_{in1} , Y_{in2} Fundamental and second-harmonic IMPATT diode input admittances; equations (1) and (2) and Fig. 1.

y_{11} , y_{22} Fundamental and second-harmonic "single-frequency" oscillator admittances; Fig. 1.

y_{12} , y_{21} Conversion transfer admittances between fundamental and second harmonic; Fig. 1.

$\bar{y}_{12}$, $\bar{y}_{21}$ Approximate form of y_{12} and y_{21}; equation (4).

α_1 , α_2 Fundamental and second-harmonic circuit admittance slope angles; Fig. 12.

γ_1 , γ_2 Fundamental and second-harmonic single-frequency diode admittance slope angles; Fig. 12.

θ_1 , θ_2 phase variables; equations (48) and (49).

θ_{10} , θ_{20} θ_1 and θ_2 for $\varphi_1 \equiv 0$, equation (13).

κ_1 , κ_2 Magnitudes of K_1 and K_2 ; equation (4).

μ Stability parameter, equation (18).

φ_1 , φ_2 Fundamental and second-harmonic voltage phases; preceding equation (1).

ψ_1 , ψ_2 Arguments of K_1 and K_2 ; equation (4).

ω_0 Fundamental radian frequency.

REFERENCES

1. Blue, J. L., "Approximate Large-Signal Analysis of IMPATT Oscillators," B.S.T.J., *48*, No. 2 (February 1969), pp. 383–396.
2. Swan, C. B., "IMPATT Oscillator Performance Improvement with Second-Harmonic Tuning," Proc. IEEE (Letter), *56*, No. 9 (September 1968), pp. 1616–1617.
3. Lee, T. P., and Standley, R. D., "Frequency Modulation of a Millimeter-Wave IMPATT Diode Oscillator and Related Harmonic Generation Effects," B.S.T.J., *48*, No. 1 (January 1969), pp. 143–161.
4. Claassen, M., and Harth, W., "Analogue-Computer Model for an Avalanche-Diode Oscillator," Electronics Letters, *5*, No. 10 (May 15, 1969), pp. 218–219.
5. Giblin, R. A., Hambleton, K. G., and Tearle, C. A., "Octave Tuning and the Effect of Second-Harmonic Loading on Avalanche-Diode Oscillators," Electronics Letters, *5*, No. 16 (August 7, 1969), pp. 361–363.

6. Mouthaan, K., and Rijpert, H. P. M., "Second-Harmonic Tuning of the Avalanche Transit-Time Oscillator," Proc. IEEE (Letters), *57*, No. 8 (August 1969), pp. 1449–1450.
7. Mouthaan, K., "Nonlinear Analysis of the Avalanche Transit-Time Oscillator," IEEE Trans. Electron Devices, *ED-16*, No. 11 (November 1969), pp. 935–944.
8. Schroeder, W. E., Greiling, P. T., and Haddad, G. I., "Multifrequency Operation of IMPATT Diodes," Int. Electron Devices Meeting, Washington, D. C., October 31, 1969.
9. Kurokawa, K., "Noise in Synchronized Oscillators," IEEE Trans. Microwave Theory and Techniques, *MTT -16*, No. 4 (April 1968), pp. 234–240.
10. Kurokawa, K., "Some Basic Characteristics of Broadband Negative Resistance Oscillator Circuits," B.S.T.J., *48*, No. 6 (July–August 1968), pp. 1937–1956.
11. Bellman, *Introduction to Matrix Analysis*, New York: McGraw-Hill, 1960, p. 245.
12. Gewartowski, J. W., and Morris, J. E., "Active Diode Parameters Obtained by Computer Reduction of Experimental Data," IEEE Trans. Microwave Theory and Techniques, *MTT-18*, No. 3 (March 1970), pp. 157–161.
13. Schlosser, W. O., "Noise in Mutually Synchronized Oscillators," IEEE Trans. Microwave Theory and Techniques, *MTT-16*, No. 9 (September 1968), pp. 732–737.